ACS OMEGA

http://pubs.acs.org/journal/acsodf

Article

# Alginate-Based Cryogels for Combined Chemo/Photothermal Antibacterial Therapy and Rapid Hemostasis

Xiao Lin, Yuxi Duan, Qian Lan, Yueying Xu, Yu Xia, Zhuoyi Huang, Lijun Song,* Yang Zhang,* and Ning Guo*

Cite This: *ACS Omega* 2023, 8, 4889−4898

Read Online

ACCESS | Metrics & More | Article Recommendations | Supporting Information

**ABSTRACT:** As novel wound dressings, cryogels with rapid hemostatic property and good sterilization effect are urgently desirable for wound healing. To reduce the use of antibiotics, antibacterial photothermal therapy with broad-spectrum bactericidal capacity and non-obvious bacterial resistance has been widely researched. However, photothermal agents usually suffer from poor hemostatic ability. In this research, sodium alginate (SA) and epigallocatechin gallate (EGCG) were non-covalently cross-linked *in suit* by ferric ions to obtain SA/EGCG/Fe (SEF) cryogels after lyophilization as an antibacterial wound dressing. Next, its photothermal performance was intensively assessed. Moreover, its hemostasis and bactericidal effect were evaluated. First, it displayed extraordinary photothermal ability owing to the formation of $Fe^{3+}$/EGCG-based metal phenolic networks (MPNs) inside the SEF cryogel. Furthermore, *in vitro* and *in vivo* assays illustrated that it exhibits rapid hemostatic capacity owing to its high porosity and MPN-mediated cell adhesion capacity. In conclusion, the SEF cryogel manifests satisfactory hemostatic and bactericidal properties. Therefore, it is a promising wound-dressing candidate for clinical applications.

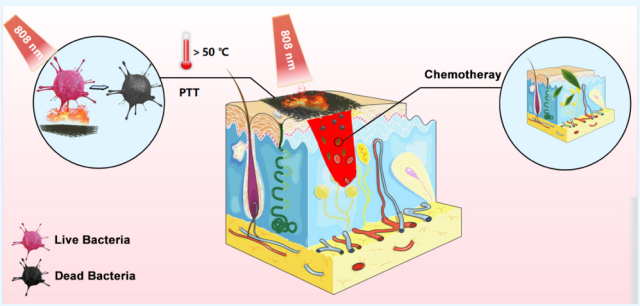


## 1. INTRODUCTION

Wound healing plays an important role in basic medical treatment and postoperative rehabilitation of clinical surgery for protecting people's life and health.[1] It is often easier to heal minor wounds, while severe traumas require medical dressing to assist in their recovery. Currently, various synthetic and natural materials, such as chitosan, sodium alginate (SA), collagen, and so on, are developed to manufacture wound dressings.[2−9] Among these materials, SA as a renewable marine biomaterial could be cross-linked with multivalent metal cations ($Ca^{2+}$, $Cu^{2+}$, and $Fe^{3+}$) to form a stable matrix.[10] Moreover, owing to its good biocompatibility, biodegradability, and hemostatic ability, SA has great application potential in inventing wound dressing platforms in clinical use.[11−13] However, SA shows no antibacterial property, and most of the patients lost their protection of skin at the wound part, which can easily cause bacterial infections, leading to serious consequences. To overcome the problem, combining with additional active ingredients (e.g., antibiotics) endows the wound dressing effective antibacterial property, but enhanced/abusive use of antibiotics causes very serious side effects and leads to drug resistance, even the creation of superbug.[14−18] Thus, it is imperative to develop more efficient SA-based wound dressing materials with antibacterial capability in a non-antibiotic way.

In recent decades, the application of non-antibiotic treatments in the field of antibacterial has attracted distinguished attention.[19−26] Unlike the antibacterial mechanism of antibiotics, there are neither adjoint toxic and adverse effects nor obtained drug resistance by using the therapeutics. Due to the inherent deep penetration, noninvasiveness, and local site targeting properties, the near-infrared (NIR)-responsive photothermal therapy (PTT) offers a promising alternative for antibacterial wound dressing fabrication.[27−31] Photothermal-active materials such as metallic compounds, carbon nanomaterials, and organic dye have been completely studied for biomedical treatments.[32−38] However, their applied exploration is limited by the high cost, tedious synthesis, low biocompatibility, and low biodegradation. Recently, metal-phenolic networks (MPNs) have been well studied to serve as a PTT platform owing to low cost and good biocompatibility.[39−41] The fabrication of MPNs was mainly based on the chelation between metal ions and the catechol structure. It suggests that the utilization of polyphenol compounds and

Received: November 7, 2022
Accepted: December 26, 2022
Published: January 27, 2023

**Scheme 1. Schematic Illustration of the Alginate-Based Cryogel and Its Application as a Combined Chemo/Photothermal Antibacterial Wound Dressing**

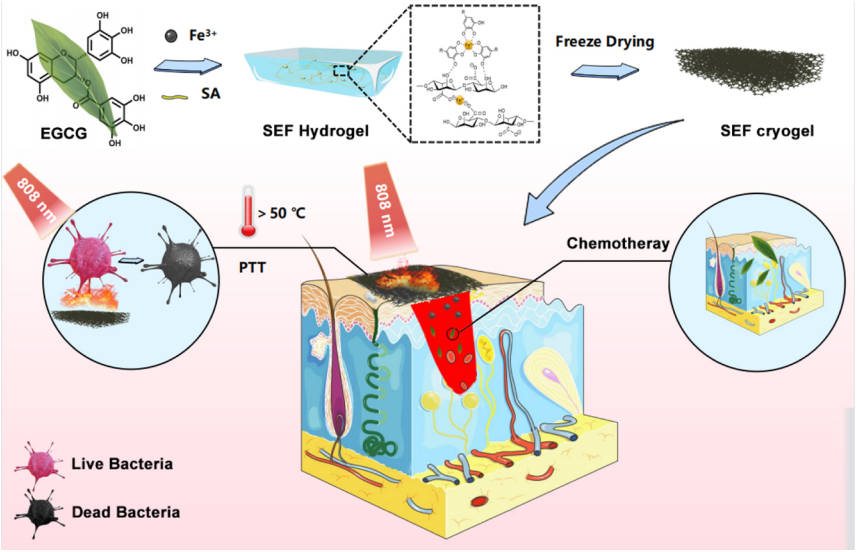


metal ions may offer an approach to the development of new photothermal materials.

Epigallocatechin gallate (EGCG) is the principal bioactive polyphenol extracted from green tea, which has antibacterial, antiviral, anti-inflammatory, and antitumor effects.[42] In addition, because of reducing inflammation by the utilization of EGCG, wound healing is accelerated obviously.[43] In this work, three natural substances including $Fe^{3+}$, SA, and EGCG were adopted to fabricate a composite cryogel as a wound dressing with excellent antibacterial function by the combination of PTT and pharmacotherapy (Scheme 1). Herein, $Fe^{3+}$ was not only cross-linked with SA to build the spongy skeleton with good blood and tissue exudate absorption capacities but also formed a photothermal chelated complex with EGCG to achieve PTT treatment. EGCG was used as a natural antimicrobial. Besides, after freeze drying, the porous scaffold of the cryogel with extremely higher water absorption capability and larger porosity was established. By the addition of the cell adhesion capacity of MPNs, the cryogel demonstrated better hemostatic performance. The experiments indicated that the cryogel shows high photothermally stimulative antibacterial performance, good hemostatic property, and favorable biocompatibility, which ensures the cryogel's great potential in clinical application for wound healing.

## 2. MATERIALS AND METHODS

**2.1. Materials.** Sodium alginate (SA), $FeCl_3{\cdot}6H_2O$, EGCG, and $CaCl_2$ were purchased from Shanghai Aladdin Biochemical Technology Co., Ltd (Shanghai, China). Mueller Hinton agar medium was purchased from Guangdong Huankai Microbial Technology Co., Ltd. (Guangdong, China). Luria−Bertani (LB) broth powder was purchased from Beijing Solarbio Biotechnology Co., Ltd. (Shanghai, China). RPMI-1640 medium and fetal bovine serum (FBS) were purchased from Gibco. Propidium iodide (PI) and SYTO 9 green fluorescent nucleic acid stain (SYTO 9) were purchased from Sigma Co., Ltd. (Shanghai, China). All solvents and reagents were analytical grade and were used as received unless declared.

**2.2. Preparation of the Cryogels.** *2.2.1. Preparation of the SA/Fe (SF) and SA/EGCG/Fe (SEF) Scaffolds.* SA and EGCG were dissolved in ultrapure water, separately. Then, the premade SA or EGCG solution was mixed in different proportions to form various concentrations [$\omega$ (SA) = 1%, C (EGCG) = 0, 0.5, 0.75 mg/mL]. After stirring for 15 min at room temperature, 4 mL of the mixture was poured into a 6-well plate, kept at 4 °C to eliminate bubbles, and then frozen at −20 °C for 12 h. The SF or SEF scaffolds were obtained by freeze-drying.

*2.2.2. Preparation of the SF and SEF Cryogels.* The SF or SEF scaffolds were first immersed into the $FeCl_3$ solution (300 mM) at 4 °C for half an hour. After that, the samples were washed with ultrapure water until colorless and kept at −20 °C for 12 h. Then, a series of SEF cryogels were obtained by freeze-drying. For example, SEF(0.5) was the sample with an SA mass fraction of 1% and the EGCG concentration of 0.5 mg/mL in the cryogel. The SF cryogel was prepared with the same procedure but without EGCG.

**2.3. Characterization.** UV−vis absorption spectra were recorded on a UV−visible spectrophotometer (UV-6000PC, Shanghai Metash Instruments Co., Ltd.). The Fourier transform infrared (FTIR) spectroscopy spectrum of cryogels SEF(0.75) was analyzed by a FTIR spectrophotometer (WQF-510A). The morphology of the prepared cryogels and the cross section of the inner structure were observed by scanning electron microscopy (SEM, JSM-IT500, JEOL, Japan). The bacteria photographs were taken by using a confocal laser scanning microscope (Leica, SP8, Germany).

**2.4. Rheological Properties of the Hydrogels.** The samples for rheological testing were prepared as previously described with some modifications. After washing with iron ions, the sample ($\Phi$ 4 × 4.5 mm) did not require to be freeze-dried. Then, the rheological test results of the cryogels were obtained by using a rheometer (TA instruments-waters-LLC, DHR-2). The elastic modulus ($G'$) and loss modulus ($G''$) were measured at a dynamic frequency sweep from 1 to 100 rad/s at 25 °C with a strain of 1%.

**2.5. Water Absorption Ability of the Cryogels.** First, the initial weight of the SF, SEF(0.5), and SEF(0.75) cryogels



https://doi.org/10.1021/acsomega.2c07170
ACS Omega 2023, 8, 4889−4898

was measured and marked as $W_0$. Then, the cryogels were immersed in ultrapure water at 37 °C for 20 min. After reaching the equilibrium swelling state, the saturated weight ($W$) of all samples was measured. The water absorption ratio was calculated according to the following equation

$$W_{WAA} = (W - W_0) / W_0 \times 100\% \quad (1)$$

**2.6. Porosity (*P*) of the Cryogels.** The porosity of the cryogels was measured in the following steps. First, the initial weight ($W_0$) of the cryogels was measured and the volume ($V$) of the cryogels was determined by the base area and the thickness. Then, the cryogels were saturated with ethanol by immersion in ethanol under reduced pressure. After 30 min, the cryogels were taken out, and the ethanol on the surface was wiped off. The weight of the ethanol-saturated cryogels was recorded as $W_1$. The porosity was calculated according to the following equation

$$P = (W_1 - W_0)/(\rho_{EtOH} \times V) \times 100\% (\rho_{EtOH} = 0.789\ g/cm^3) \quad (2)$$

**2.7. Release of EGCG in the SEF Cryogels.** The release performance of the cryogels was evaluated by measuring the amount of EGCG released under different conditions. The specific steps were as following. First, 10 mg of cryogel powder was placed in a 5 mL PBS (PH = 7.4, PH = 5.5) system and reacted in a water bath at 37 °C. At given intervals, all 10 mL of PBS in the system was removed for determination and supplemented with 10 mL of fresh buffer. The cumulative release was calculated according to the EGCG standard curve.

**2.8. Photothermal Properties of the SEF Cryogels.** The cryogel was first put into an EP tube with 1 mL ultrapure water and then irradiated by an 808 nm laser (0.5 W/cm$^2$) for 10 min. During the process, a Fluke TiS75 thermal imager camera was used to capture the thermal images at a time interval of 30 s. The temperature was read from the thermal images and used to evaluate the photothermal properties of the cryogel.

The photothermal repeatability of the cryogel was estimated by repeated heating and cooling processes 10 times. The cooling process was operated by turning off the NIR laser to allow cooling to room temperature naturally. The heating process and data collection were performed as previously described. Photothermal conversion efficiency was calculated according to previous reports.[41]

**2.9. Bacteria Culture.** *Staphylococcus aureus* (ATCC 25923) and *Escherichia coli* (ATCC 25922) were generously gifted by Guangzhou Institute of Microbiology. The single colony of bacteria was suspended in an LB medium and then incubated at 37 °C under 220 rpm shaking for 12 h. The logarithmic growth bacteria were obtained by centrifugation and re-suspended in fresh LB medium.

**2.10. *In Vitro* Antibacterial Experiments of the SEF Cryogels.** *E. coli* and *S. aureus* were used as the test model bacteria to evaluate the *in vitro* antibacterial activities of the cryogels. Before each experiment, all samples and instruments were sterilized by ultraviolet light irradiation for 30 min. Then, the cryogels (Φ 8 × 2 mm) were placed on the bottom of a 48-well plate, and 0.5 mL of bacterial suspension (10$^8$ CFU/mL) was added to each well. The samples were divided into NIR group and non-NIR group. For the NIR group, each well was subjected to an 808 nm laser (0.5 W/cm$^2$) for 10 min, after which 0.5 mL of LB medium was added to each well (including the non-NIR group). Finally, the plates were cultured at 37 °C for 12 h, and the absorbance of the suspension at 600 nm ($OD_{600}$) was measured to evaluate the viability of the bacteria.

After the antibacterial test, the same sample was used to perform an antibacterial test again to evaluate the antibacterial repeatability of the cryogel. The antibacterial experiments were performed as described above. But after each test, the cryogels were taken out and soaked in ethanol, washed several times with ultrapure water, and lyophilized. Then, the lyophilized used samples were irradiated with ultraviolet light for 30 min and dealt with bacteria again. The process was repeated at least three times.

**2.11. Fluorescence Microscopic Observation (Live/Dead).** The cryogels were cultured with 0.5 mL bacteria dispersion (10$^8$ CFU/mL) at 37 °C for 3 h. Then, the samples were randomly divided into NIR group and non-NIR group. For the NIR group, each sample was subjected to an 808 nm laser (0.5 W/cm$^2$) for 10 min. Subsequently, the bacteria were washed twice with PBS and collected by centrifuging at 5000 rpm for 5 min. The working solution was prepared by mixing 0.6 μL SYTO 9, 10 μL PI, and 990 μL PBS together. Then, 300 μL of the working solution was incubated with the obtained bacterial pellet in dark at 37 °C for 20 min. Finally, all of the bacteria were stained for green color by SYTO 9, but the dead bacteria were stained for red color by PI. All samples were fixed with 2.5% glutaraldehyde solution and imaged by CLSM.

**2.12. Cytotoxicity Experiments of the Cryogels.** L929 mouse fibroblasts were obtained from the Cell Bank of the Chinese Academy of Sciences and used in all the cell culture tests. Generally, the cells were cultured with RPMI-1640 medium at 37 °C under an atmosphere containing 5% $CO_2$. The medium contained 10% FBS (Gibco) and 1% penicillin streptomycin. To assess the cytotoxicity, various cryogel powders were co-cultured with L929 cells overnight at 37 °C. The cells were then treated with the methylthiazolyldiphenyl-tetrazolium bromide (MTT) solution, and the absorbance of the mixture was measured at 570 nm ($A570_{test}$) to evaluate the biocompatibility of the cryogel. The L929 cells without any treatment were used as the control group ($A570_{control}$), and the cell survival rate was calculated by the following formula

$$\text{Cell survival rate}(\%) = A570_{test}/A570_{control} \times 100\% \quad (3)$$

Cell proliferation was assessed by co-cultivating L929 cells on the surface of the cryogels with various concentrations. Before the experiment, all the cryogels (Φ 8 × 1 mm) were irradiated with ultraviolet rays for 30 min. Then, the sterile cryogels were laid in a 48-well plate, and 1 mL of L929 cells with a density of 1 × 10$^5$ cells/mL was added. The cells were cultured at 37 °C for 1 day and 3 days, respectively. Afterward, 50 μL of MTT solution was added to each well and incubated for 4 h at 37 °C. After removing the medium, a purple solution was obtained by adding 500 μL of dimethyl sulfoxide (DMSO). 200 μL of the purple solution was filled into a 96-well plate, and the absorbance at 570 nm ($OD_{570}$) was measured by a microplate reader.

**2.13. Hemostatic Experiments of the Cryogels.** The hemostatic capacities of the cryogels were studied by the rat-tail cutting experiment. All animal experiments were approved by the Animal Ethics Committee of Guangdong Medical University. And all animal experiments were conducted in accordance with the guidelines of the Institutional Animal Care


https://doi.org/10.1021/acsomega.2c07170
ACS Omega 2023, 8, 4889−4898

and Use Committee at Guangdong Medical University. Male Sprague-Dawley (SD) rats (180−200 g) were purchased from Guangdong Provincial Animal Center (Guangzhou, China) and kept in the SPF animal house. The experiment consisted of four groups, each containing 3 SD rats. Briefly, 30% length of the rats' tails was cut off and quickly wrapped with gauze, SA, and SEF cryogels. Then, the weight of blood loss and the hemostasis time were recorded to evaluate the hemostatic capacities of the cryogels.

**2.14. Blood Cell Adhesion Experiments of the Cryogels.** 100 $\mu$L of whole blood was dropped onto the gauze and the cryogels [SF and SEF(0.75)], respectively, for incubation of 5 min at 37 °C. The unattached blood cells were washed away by PBS, and the adhered cells were fixed with 2.5% glutaraldehyde for 3 h. Afterward, the cryogels were dehydrated by ethanol-aqueous solutions with a gradient concentration (50, 60, 70, 80, 90, and 100%). Finally, the morphology of the treated samples was observed by SEM.

**2.15. Blood-Clotting Index of the Cryogels.** All the cryogels [SF and SEF(0.75)] were cut into cylindrical specimens of the same size (Φ 8 × 5 mm). Then, 100 $\mu$L of recalcified blood-aqueous solution (10 mM $CaCl_2$) was dropped on to the surfaces of the cryogels. All the samples were incubated at 37 °C for 2.5 min, and 10 mL of deionized (DI) water was carefully added without disturbing the clotted blood. The absorbance of the supernatant at 540 nm ($A540_{test}$) was recorded by a microplate reader. The absorbance of the mixture of blood (100 $\mu$L) and DI water (10 mL) was used as the control group ($A540_{control}$). The blood-clotting index (BCI) was calculated according to the following formula

$$BCI(\%) = (A540_{test}/A540_{control}) \times 100\% \quad (4)$$

**2.16. *In Vivo* Wound-Healing Performance of the Cryogels.** All animal experiments have been approved by the Animal Ethics Committee of Guangdong Medical University. The wound-healing performance of the cryogel was evaluated by using a wound infection model on Sprague−Dawley rats (SD, male, Guangdong Animal Experimental Center, 230−270 g), which were randomly divided into six groups (Control, Control + NIR, SF, SF + NIR, SEF, and SEF + NIR). Each group contained 3 SD rats. The back skin of the rats was exposed by shaving the hair, and a hole with a diameter of 8 mm was punched. Then, 10 $\mu$L of *S. aureus* solution ($10^{10}$ CFU/mL) was dropped on the wound area for 30 min. The cryogels (Φ 8 × 2.5 mm) were placed on the wound site. The NIR-treated groups were irradiated for 10 min. The wound conditions of the rats were monitored on the 0th, 5th, and 10th day, and the wound size was recorded.

**2.17. Statistical Analysis.** The data were collected in three parallel experiments, and the values were indicated as the mean ± standard deviation (SD). Student's *t*-test was used to conclude the statistical analysis. In all tests, the level of statistical significance was set at $*p < 0.05$, $**p < 0.01$, and $***p < 0.001$.

## 3. RESULTS AND DISCUSSION

**3.1. Synthesis and Characterization of the SEF Cryogels.** The composite cryogels were fabricated by a simple and facile method (Scheme 1). Briefly, the solitary SA or the mixture of EGCG and SA was freeze-dried to obtain the intermediates, which were immersed in a ferric ion solution and lyophilized again to acquire the final products. All the samples were named according to their composition for convenience. For instance, the matrix without and with EGCG were labeled as SA/Fe (SF) and SA/EGCG/Fe (SEF), respectively. In addition, the SEF(0.5) represented that the concentration of EGCG was 0.5 mg/mL. In order to verify the successful fabrication of SEF cryogels, the FTIR spectroscopy of SA, EGCG, and SEF(0.75) was adopted. As shown in Figure 1a, the peaks at 1650 and 1570 $cm^{-1}$ in the EGCG spectrum

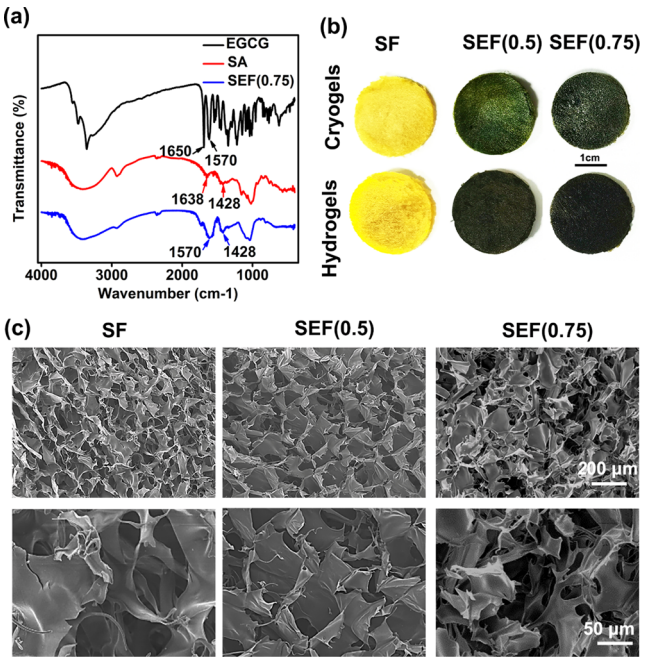


**Figure 1.** (a) FTIR spectrometry of SA, EGCG, and SEF(0.75). (b) Photographs of cryogels and hydrogels. (c) Morphology of gauze and cryogels determined by SEM. Scale bar: 200 and 50 $\mu$m.

were, respectively, attributed to C═O and C═C groups. The peaks at 1638 and 1428 $cm^{-1}$ in the SA spectrum were, respectively, attributed to C═O and C−O groups. However, in the SEF(0.75) spectrum, the peak at 1570 $cm^{-1}$ corresponding to the C═C group of EGCG and the peak at 1428 $cm^{-1}$ corresponding to the C−O group of SA emerged, indicating the successful preparation of SEF cryogels. The color of the cryogels turned from yellow to black while EGCG was added, which was attributed to the dark EGCG/$Fe^{3+}$ complex (Figure 1b). After water absorption, the diameter of all obtained hydrogels showed a much low increase, which was favorable to decrease the compressive stress to surrounding tissues (Figure 1b). The morphology of freeze-dried cryogels was observed by SEM, and the images in Figure 1c show that SF- and EGCG-doped SEF cryogels had a similar loose flake structure with interconnected pores. As a result, the porous scaffold endowed the cryogels with extremely higher water absorption capability and larger porosity.

A rheometer was employed to evaluate the rheological properties of the SF and SEF hydrogels. As exhibited in Figure 2a, the storage modulus ($G'$) values are bigger than the loss modulus ($G''$) values for all the three hydrogels, which demonstrated that the hydrogels could stay stable for a long period. Compared with the SF hydrogel, the degree of cross-linking in SEF hydrogels was higher owing to the addition of EGCG and formation of MPNs. As a result, the $G'$ values of SEF hydrogels are greater than those of SF hydrogels. As shown in Figure 2b, the SF and SEF cryogels possessed


https://doi.org/10.1021/acsomega.2c07170
ACS Omega 2023, 8, 4889−4898

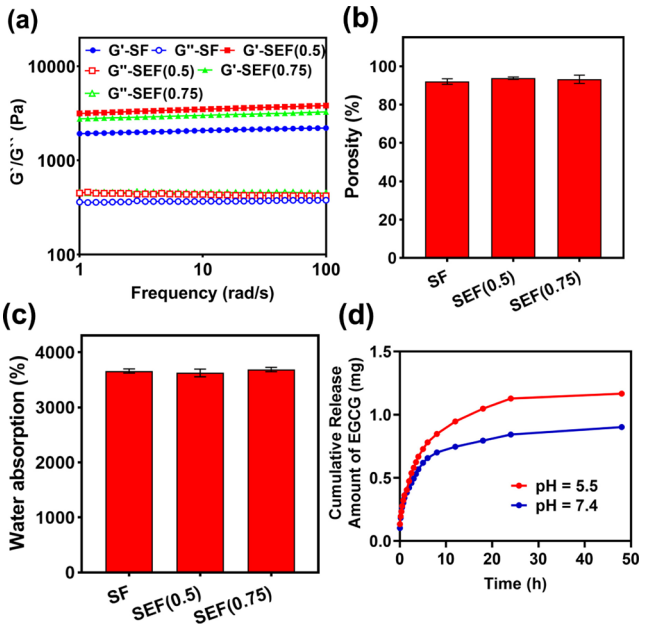


**Figure 2.** (a) Storage modulus ($G'$) and loss modulus ($G''$) curves of hydrogels. (b) Water absorption rates and (c) porosity rates of cryogels. (d) Release of EGCG from SEF(0.75) at pH 5.5 and 7.4.

abnormally high porosity values that exceeded 92%. Due to the high-value porosity of skeletons and the excellent hydrophilicity of SA, high water absorption ratios (about 3600%) of all the cryogels were obtained. It was beneficial for the scaffolds to absorb tissue exudates and maintain the appropriate moisture environment at the wound, so as to accelerate wound healing (Figure 2c). Since EGCG was used as an antibacterial agent in this system, the release features of EGCG from the SEF(0.75) cryogel were studied at pH 5.5 and 7.4. As shown in Figure 2d, the release amount of EGCG at pH 5.5 was obviously higher than that at pH 7.4 after 48 h, representing a pH-responsive release behavior. Thus, more EGCG could be released from the SEF cryogel at the infectious tissues (pH ≈ 5.5), which would enhance the antibacterial effect of the SEF cryogel.

**3.2. Photothermal Property of the SEF Cryogels.** As we hypothesized that the complexes of polyphenols and metal cations could be exploited for developing new PTT agents, the photothermal capacity of the cryogels was measured and is displayed in Figure 3. After 10 min exposure to the NIR laser (808 nm, 0.5 W/cm$^2$), the temperature of SF cryogel only increased by 11 °C (Figure 3b). However, upon adding EGCG, the EGCG/$Fe^{3+}$-based MPNs were formed and the photothermal effects of SEF cryogels were obviously promoted. The temperature of the SEF cryogel could increase by at least 26 °C under irradiation for 10 min. By increasing the amount of EGCG, the maximum attainable temperature could rise from 26 to 37 °C (Figure 3b). Then, the SEF(0.75) cryogel was chosen as a typical representative sample to elucidate further photothermal characteristics. Moreover, the temperature of SEF cryogels exhibited a laser-power-dependent manner (Figure 3c). Furthermore, there was no noticeable change in the temperature of cryogels after undergoing 10 cycles of NIR irradiation (0. 5 W/cm$^2$, 10 min), demonstrating the excellent photothermal stability of SEF cryogels (Figure 3d).

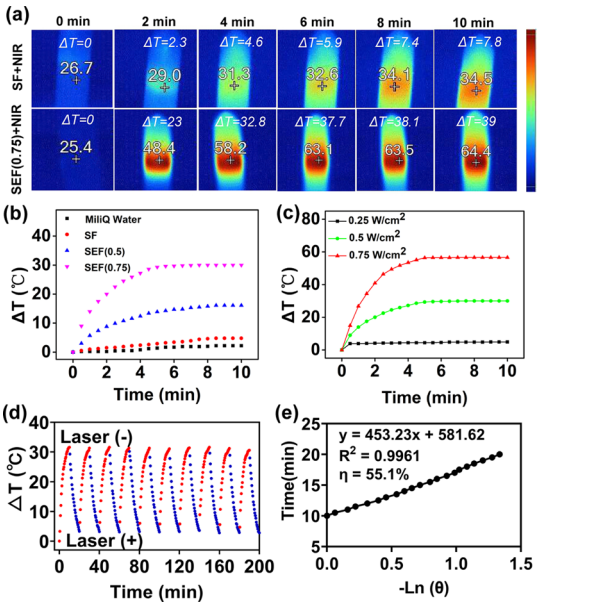


**Figure 3.** (a) Infrared thermal images of SF and SEF(0.75) cryogels under NIR irradiation (808 nm, 0.5 W/cm$^2$) at different time points. Temperature changes of cryogel aqueous solutions under NIR laser irradiation (b) treated with different cryogels (808 nm, 0.5 W/cm$^2$, 10 min), (c) at different power densities [SEF(0.75)]. (d) Heating and cooling curves of the SEF(0.75) aqueous solution over 10 cycles of irradiation (808 nm, 0.5 W/cm$^2$, 10 min). (e) Time constant obtained by applying the linear fit of time from the cooling period *vs* −ln ($\theta$).

**3.3. *In Vitro* Antibacterial Property the SEF Cryogels.** The photothermal antimicrobial properties of the cryogels were first evaluated by detecting the growth reduction of Gram positive (*S. aureus*) and negative (*E. coli*) bacteria both with and without NIR irradiation. As shown in Figure 4a,b, only

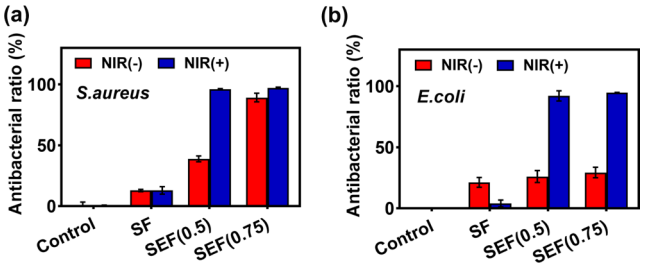


**Figure 4.** Antibacterial rates of (a) *S. aureus* and (b) *E. coli* after different treatments.

small amounts of *E. coli* and *S. aureus* were eliminated by the SF scaffold with or without NIR illumination, demonstrating its weak antibacterial effect. It is well known that EGCG could be used as an effective antibacterial agent. While EGCG was integrated with SF, the SEF cryogels showed an enhanced antibacterial effect in the dark. Furthermore, the higher bacteriostatic rates of the SEF cryogels were inspiringly observed after exposure to NIR for 10 min. Nearly 95% of *E. coli* and 97% of *S. aureus* were killed, which indicated the excellent photothermal antibacterial ability of the EGCG-doped cryogels.

We also used a fluorescence microscope to intuitively observe the viability of both *E. coli* and *S. aureus*. The CLSM images are displayed in Figure 5, in which all bacterial cells were labeled green by SYTO 9, while the dead ones were


https://doi.org/10.1021/acsomega.2c07170
ACS Omega 2023, 8, 4889−4898

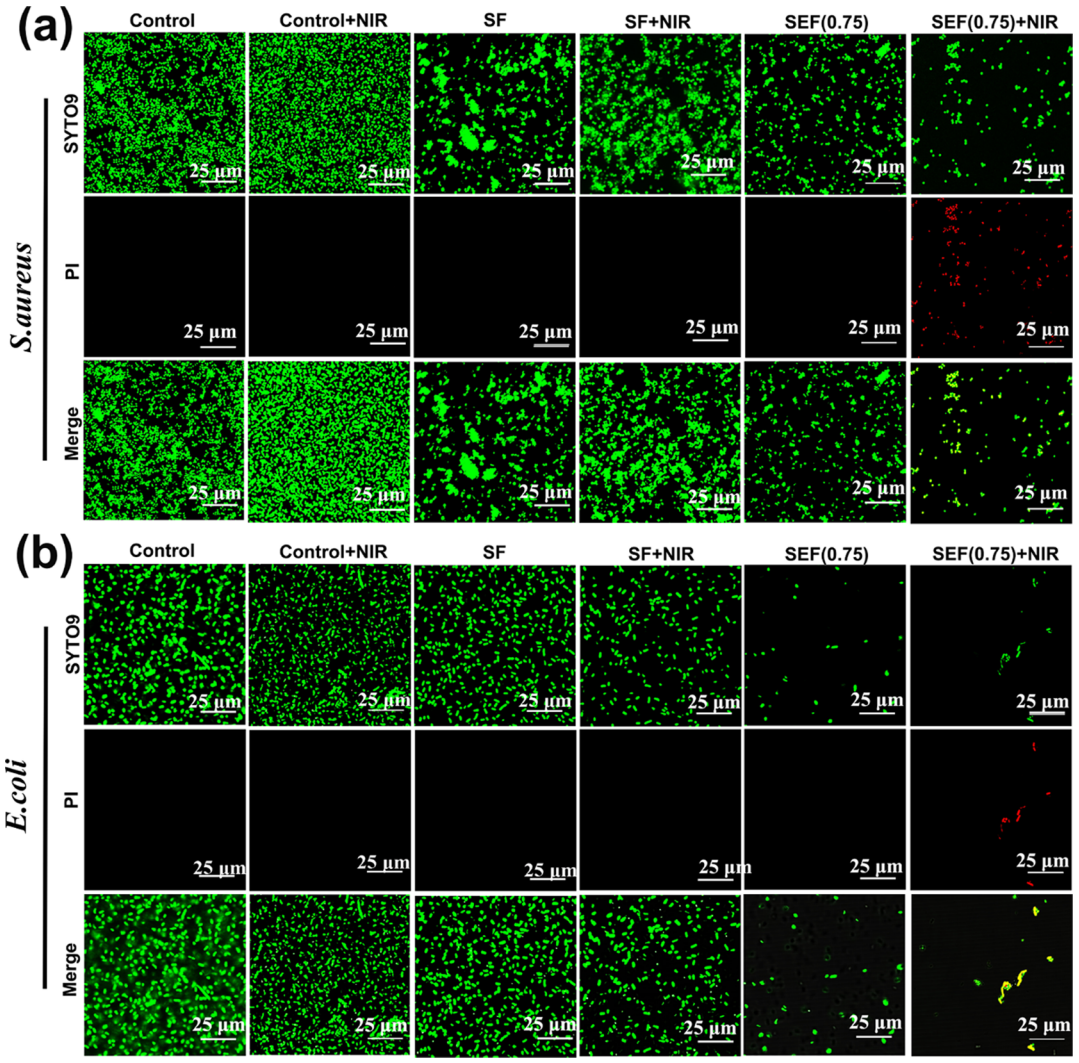


**Figure 5.** Confocal laser scanning microscopy images of (a) *S. aureus* and (b) *E. coli*, where dead/live bacteria are labeled green by SYTO 9 and dead bacteria are labeled red by PI (scale bar: 25 $\mu$m).

marked red by PI. It was obviously found that the red spots emerged in the group of the bacteria incubated with the cryogels containing EGCG after NIR irradiation, demonstrating the excellent photothermal bacterial-killing efficiency. These outcomes are in accordance with the results obtained from the antibacterial assays.

Besides, the antimicrobial efficiency of SEF(0.75) was still higher than 80% against both *S. aureus* and *E. coli* even after 3 cycles of NIR illumination, which benefited from its repeatable photothermal property (Figure 6a,b).

**3.4. Cell Biocompatibility of the SEF Cryogels.** For wound-healing materials, their biosafety should be considered as the prerequisite for practical applications. After treating L929 with the cryogels for 24 h, the cell viabilities of all groups were higher than 85%, indicating excellent biocompatibility of the cryogels (Figure 7a). As reported, EGCG could promote the mammalian cell proliferation. Furthermore, the cell proliferation activity of the cryogels was also evaluated by dispersing L929 cell suspensions on the surface of SF, SEF(0.5), and SEF(0.75) for a culture period of 1 or 3 days, separately. As shown in Figure 7b, the OD values of EGCG-loaded cryogels were obviously higher than those of the SF scaffold after 1 day. After 3 days, the enlarged trend of the

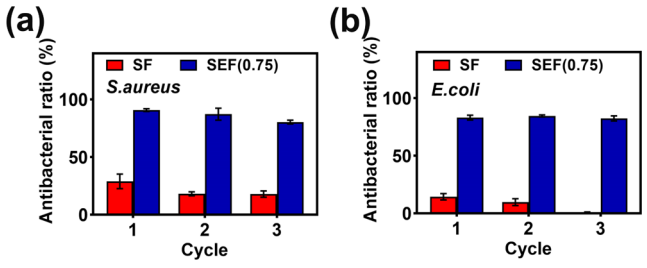


**Figure 6.** Antibacterial rates of the SEF(0.75) cryogel against (a) *S. aureus* and (b) *E. coli* under NIR irradiation (808 nm, 0.5 W/cm$^2$, 10 min) for 3 cycles.

difference in cell proliferation confirmed the enhanced cell proliferation.

**3.5. Hemostatic Property of the SEF Cryogels.** Hemostatic ability is important for wound dressings in preventing excessive post-traumatic bleeding. In our research, cutting tail test of SD male rats was used to assess the hemostatic capacities of the cryogels (Figure 8a). During the experiments, the blood loss and hemostatic time of the gauze, SF cryogel, and SEF cryogel were recorded, respectively. Compared to the gauze, both a less blood loss and shorter



https://doi.org/10.1021/acsomega.2c07170
ACS Omega 2023, 8, 4889−4898

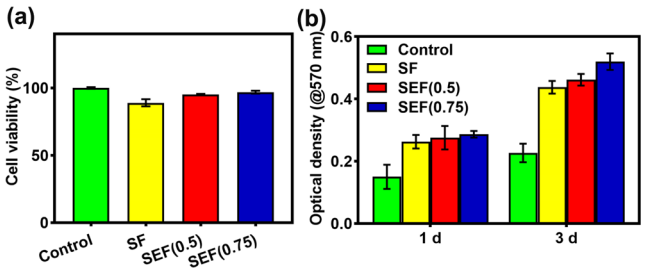


**Figure 7.** (a) Cell viability of L929 cells incubated with cryogels for 24 h. (b) Optical density values of different concentrations of cryogels incubated with L929 cells for 1 day and 3 days, respectively.

hemostatic time were caused by SA cryogels attributed to its inherent higher water absorption capability and larger porosity. Interestingly, the blood loss and hemostatic time were further dramatically diminished through employing the SEF cryogel, which illustrates the cell adhesion property of MPNs.[44−46] Owing to the extraordinary hemostatic ability of the SEF(0.75) cryogel, the blood loss and hemostasis time were diminished by 91.49 and 84.74% in comparison with the gauze (Figure 8b,c).

To further study the hemostasis mechanism of the SEF cryogel, blood cell adhesion assay was conducted by dropping the whole blood onto the gauze, SF cryogel, and SEF cryogel, separately. After incubation and fixation, the obtained specimens were characterized by SEM to view the adhesion geometry and morphology of RBCs, respectively. As illustrated in Figure 8d, few blood cells adhered onto the surface of the gauze. For the SF cryogel, increased blood cell adhesion was observed. Notably, the amount of adhered blood cells with a regular disk morphology on the surface of the SEF(0.75) cryogel was dramatically enhanced compared to the SF cryogel and gauze, which can be attributed to the cell adhesion capacity of MPNs.[43] In addition, values of BCI were measured by dropping RBC suspensions on the gauze, SF cryogel, and SEF cryogel, respectively. After incubation, the values of BCI were calculated, separately (Figure 8e). Expectedly, the value of BCI for the SEF cryogel (14.95%) is much less than that of the gauze (82.08%), which proved its excellent blood-clotting capacity. Therefore, all these inspiring experimental outcomes indicated the excellent tissue exudate absorption and blood clotting capacities of the SEF cryogel to be employed as a promising candidate for wound dressing in future clinical trials.

**3.6. *In Vivo* Wound-Healing Performance of the Cryogels.** As *in vitro* experiments demonstrated the efficient antibacterial ability, satisfactory hemostatic capability, and good biocompatibility of the SEF cryogel, we built the *S. aureus*-infected trauma model on the back skin of SD mice to further assess the *in vivo* therapeutic effect of the cryogels. After infection, all the infected SD mice were divided randomly into six groups: (1) Control, (2) Control + NIR, (3) SF, (4) SF +

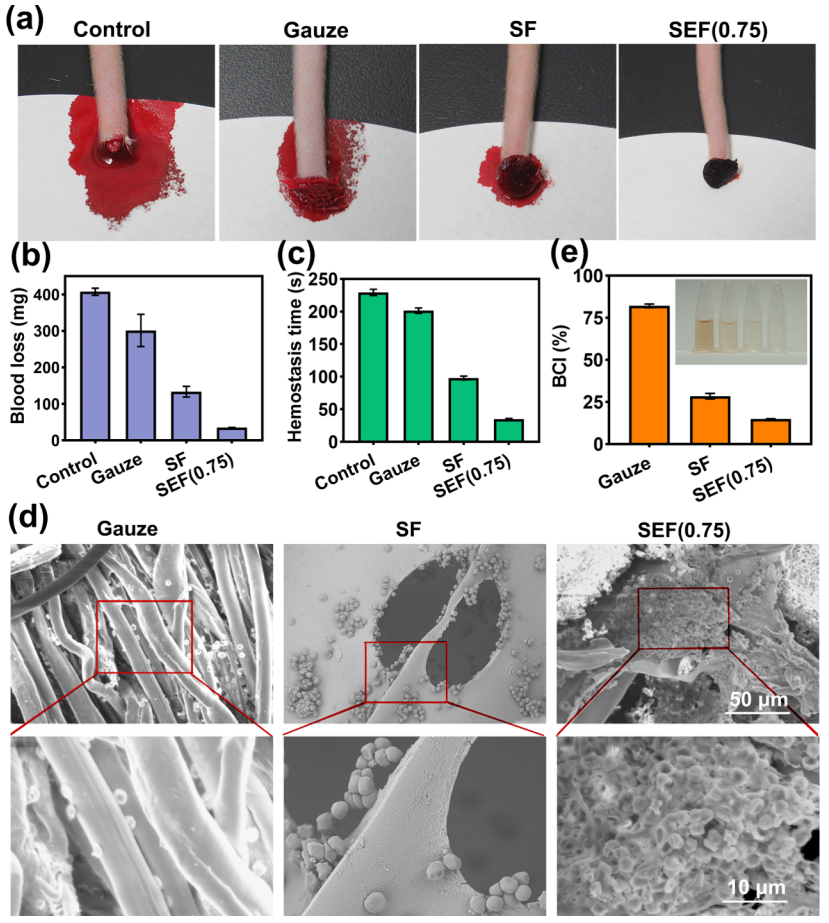


**Figure 8.** (a) Images of hemostasis by using the gauze, SF cryogel, and SEF(0.75) cryogel. (b) Blood loss and (c) hemostatic time on the truncated rat-tail model by using the gauze, SF cryogel, and SEF(0.75) cryogel. (d) SEM images of the blood red cell adhesion on the gauze, SF cryogel, and SEF(0.75) cryogel. (e) Whole blood clotting evaluation of the gauze, SF cryogel, and SEF(0.75) cryogel.



https://doi.org/10.1021/acsomega.2c07170
*ACS Omega* 2023, 8, 4889−4898

NIR, (5) SEF, and (6) SEF + NIR. Subsequently, SF and SEF cryogels were dressed on the infection site with or without NIR illumination (808 nm, 0.5 W/cm$^2$, 10 min), respectively. 10 days later, the mice were sacrificed after treatments. Through wound closure evaluation, it was found that the SEF cryogel achieved a greatly accelerated healing rate compared to the SF cryogel on day 5 due to the wound-healing-promoting property of EGCG (Figures 9 and S1). After 10 days, the

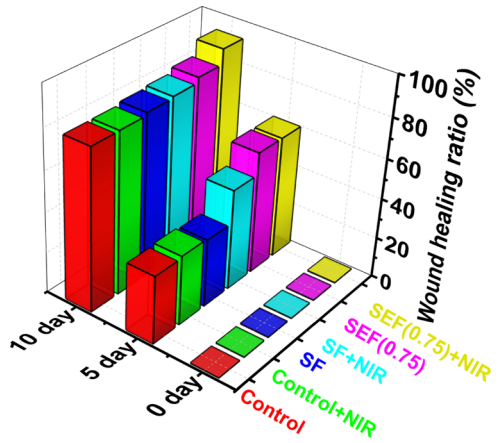


**Figure 9.** Wound healing ratio of different treatments.

group treated with SEF cryogel and NIR represented the highest wound-healing rate, which proved that the SEF cryogel had a good ability to promote the healing process of the bacterial-infected trauma. Hence, these *in vivo* results solidly illustrated the satisfactory hemostatic, antibacterial, and wound-healing-accelerating capacities of the SEF cryogel, which has great potential to be applied in clinical treatments in future.

## 4. CONCLUSIONS

In conclusion, a novel non-antibiotic based antimicrobial wound dressing, SEF cryogel, has been successfully prepared for rapid hemostasis and combined chemo/photothermal therapy against bacterial infection. The SEF cryogel was synthesized by the lyophilization of *in suit* non-covalently cross-linked hydrogel, which consists of SA, EGCG, and ferric ions. Due to excellent photothermal effect of MPNs, *in vitro* antibacterial experiments illustrated that the sterilization effect of SEF cryogel was significantly enhanced under NIR irradiation to achieve a combined chemo/PTT. Additionally, both the inherent high porosity of cryogels and cell adhesion capacity of MPNs benefit tissue exudate absorption and rapid hemostasis. Finally, both *in vitro* and *in vivo* tests demonstrated its satisfactory biosafety, hemostatic abilities, and wound-healing-accelerating capacities for bacterial infection. Therefore, this multifunctional cryogel has great potential to be employed as a candidate for wound dressing for clinical trials in future.

## ■ ASSOCIATED CONTENT

### Supporting Information

The Supporting Information is available free of charge at https://pubs.acs.org/doi/10.1021/acsomega.2c07170.

*In vivo* assessment of cryogels for wound healing (PDF)

## ■ AUTHOR INFORMATION


### Corresponding Authors

**Lijun Song** − *School of Pharmacy, Institute of Traditional Chinese Medicine and New Pharmacy Development, Guangdong Medical University, Dongguan 523808, China*; Email: songlijun6981@126.com

**Yang Zhang** − *South China Institute of Collaborative Innovation, Dongguan 523808, China; Guangdong Dongguan Quality Supervision Testing Center, Dongguan 523808, China*; Email: zyxx2010@163.com

**Ning Guo** − *School of Pharmacy, Institute of Traditional Chinese Medicine and New Pharmacy Development, Guangdong Medical University, Dongguan 523808, China*; orcid.org/0000-0001-8920-1236; Email: guoning19890501@163.com

### Authors

**Xiao Lin** − *School of Pharmacy, Institute of Traditional Chinese Medicine and New Pharmacy Development, Guangdong Medical University, Dongguan 523808, China*

**Yuxi Duan** − *School of Pharmacy, Institute of Traditional Chinese Medicine and New Pharmacy Development, Guangdong Medical University, Dongguan 523808, China*

**Qian Lan** − *School of Pharmacy, Institute of Traditional Chinese Medicine and New Pharmacy Development, Guangdong Medical University, Dongguan 523808, China*

**Yueying Xu** − *School of Pharmacy, Institute of Traditional Chinese Medicine and New Pharmacy Development, Guangdong Medical University, Dongguan 523808, China*

**Yu Xia** − *School of Pharmacy, Institute of Traditional Chinese Medicine and New Pharmacy Development, Guangdong Medical University, Dongguan 523808, China*

**Zhuoyi Huang** − *School of Pharmacy, Institute of Traditional Chinese Medicine and New Pharmacy Development, Guangdong Medical University, Dongguan 523808, China*

Complete contact information is available at: https://pubs.acs.org/10.1021/acsomega.2c07170


### Author Contributions

X.L., Y.D., and Q.L. contributed equally to this work. Conceptualization: L.S., Y.Z., and N.G.; methodology: X.L., Y.D., and Q.L.; investigation: X.L., Y.D., Q.L., Y.Y.X., Y.X., and Z.H.; data curation, X.L., Y.D., and Q.L.; writing—original draft preparation: X.L., Y.Z., and N.G.; writing—review and editing: L.S., Y.Z., and N.G.; supervision: L.S., Y.Z., and N.G.; project administration: X.L.,Y.Z., and N.G.; funding acquisition: S.L., Y.Z., and N.G.. All authors have read and agreed to the published version of the manuscript.


### Funding

This research was financially supported by the Guangdong Basic and Applied Basic Research Foundation (2020A1515110344), Innovation Program of Zhanjiang (2020LHJH005), Key Project of Social Science and Technology Development of Dongguan (no. 20185071521658), and Discipline Construction Project of Guangdong Medical University (1015KPGYF20210026).


### Notes

The authors declare no competing financial interest.

## ■ REFERENCES


(1) Childs, D. R.; Murthy, A. S. Overview of Wound Healing and Management. *Surg. Clin. North Am.* **2017**, *97*, 189−207.

(2) Brindha, J.; Chanda, K.; Balamurali, M. M. Revisiting the insights and applications of protein engineered hydrogels. *Mater. Sci. Eng. C* **2019**, *95*, 312−327.
(3) Jing, X.; Sun, Y.; Ma, X.; Hu, H. Marine polysaccharides: green and recyclable resources as wound dressings. *Mater. Chem. Front.* **2021**, *5*, 5595−5616.
(4) Liang, W.; Lu, Q.; Yu, F.; Zhang, J.; Xiao, C.; Dou, X.; Zhou, Y.; Mo, X.; Li, J.; Lang, M. A multifunctional green antibacterial rapid hemostasis composite wound dressing for wound healing. *Biomater. Sci.* **2021**, *9*, 7124−7133.
(5) Pourjabbar, B.; Biazar, E.; Heidari Keshel, S.; Baradaran-Rafii, A. Improving the properties of fish skin collagen/silk fibroin dressing by chemical treatment for corneal wound healing. *Int. Wound J.* **2022**, 1−15, DOI: 10.1111/iwj.13896.
(6) Wu, X.; Li, H. Incorporation of Bioglass Improved the Mechanical Stability and Bioactivity of Alginate/Carboxymethyl Chitosan Hydrogel Wound Dressing. *ACS Appl. Bio Mater.* **2021**, *4*, 1677−1692.
(7) Xia, J.; Zhang, H.; Yu, F.; Pei, Y.; Luo, X. Superclear, Porous Cellulose Membranes with Chitosan-Coated Nanofibers for Visualized Cutaneous Wound Healing Dressing. *ACS Appl. Mater. Interfaces* **2020**, *12*, 24370−24379.
(8) Yao, Y.; Zhang, A.; Yuan, C.; Chen, X.; Liu, Y. Recent trends on burn wound care: hydrogel dressings and scaffolds. *Biomater. Sci.* **2021**, *9*, 4523−4540.
(9) Huang, Y.; Bai, L.; Yang, Y.; Yin, Z.; Guo, B. Biodegradable gelatin/silver nanoparticle composite cryogel with excellent antibacterial and antibiofilm activity and hemostasis for Pseudomonas aeruginosa-infected burn wound healing. *J. Colloid Interface Sci.* **2022**, *608*, 2278−2289.
(10) Hu, C.; Lu, W.; Mata, A.; Nishinari, K.; Fang, Y. Ions-induced gelation of alginate: Mechanisms and applications. *Int. J. Biol. Macromol.* **2021**, *177*, 578−588.
(11) Peng, W.; Li, D.; Dai, K.; Wang, Y.; Song, P.; Li, H.; Tang, P.; Zhang, Z.; Li, Z.; Zhou, Y.; Zhou, C. Recent progress of collagen, chitosan, alginate and other hydrogels in skin repair and wound dressing applications. *Int. J. Biol. Macromol.* **2022**, *208*, 400−408.
(12) Varaprasad, K.; Jayaramudu, T.; Kanikireddy, V.; Toro, C.; Sadiku, E. R. Alginate-based composite materials for wound dressing application:A mini review. *Carbohydr. Polym.* **2020**, *236*, 116025.
(13) Zhang, M.; Zhao, X. Alginate hydrogel dressings for advanced wound management. *Int. J. Biol. Macromol.* **2020**, *162*, 1414−1428.
(14) Liu, W.; Wang, M.; Cheng, W.; Niu, W.; Chen, M.; Luo, M.; Xie, C.; Leng, T.; Zhang, L.; Lei, B. Bioactive antiinflammatory antibacterial hemostatic citrate-based dressing with macrophage polarization regulation for accelerating wound healing and hair follicle neogenesis. *Bioact. Mater.* **2021**, *6*, 721−728.
(15) Lozeau, L. D.; Grosha, J.; Smith, I. M.; Stewart, E. J.; Camesano, T. A.; Rolle, M. W. Alginate Affects Bioactivity of Chimeric Collagen-Binding LL37 Antimicrobial Peptides Adsorbed to Collagen-Alginate Wound Dressings. *ACS Biomater. Sci. Eng.* **2020**, *6*, 3398−3410.
(16) Qian, Z.; Bai, Y.; Zhou, J.; Li, L.; Na, J.; Fan, Y.; Guo, X.; Liu, H. A moisturizing chitosan-silk fibroin dressing with silver nanoparticles-adsorbed exosomes for repairing infected wounds. *J. Mater. Chem. B* **2020**, *8*, 7197−7212.
(17) Rai, A.; Ferrão, R.; Marta, D.; Vilaça, A.; Lino, M.; Rondão, T.; Ji, J.; Paiva, A.; Ferreira, L. Antimicrobial Peptide-Tether Dressing Able to Enhance Wound Healing by Tissue Contact. *ACS Appl. Mater. Interfaces* **2022**, *14*, 24213−24228.
(18) Zhao, X.; Liu, L.; An, T.; Xian, M.; Luckanagul, J. A.; Su, Z.; Lin, Y.; Wang, Q. A hydrogen sulfide-releasing alginate dressing for effective wound healing. *Acta Biomater.* **2020**, *104*, 85−94.
(19) Li, C.; Li, Z.; Zeng, Y.; Cao, X.; Zhao, H.; Yang, Y. Y.; Yuan, P.; Lu, X.; Ding, X. Co3 O4 Nanowires Capable of Discharging Low Voltage Electricity Showing Potent Antibacterial Activity for Treatment of Bacterial Skin Infection. *Adv. Healthcare Mater.* **2022**, *11*, No. e2102044.
(20) Li, M.; Qiu, W.; Wang, Q.; Li, N.; Liu, L.; Wang, X.; Yu, J.; Li, X.; Li, F.; Wu, D. Nitric Oxide-Releasing Tryptophan-Based Poly(ester urea)s Electrospun Composite Nanofiber Mats with Antibacterial and Antibiofilm Activities for Infected Wound Healing. *ACS Appl. Mater. Interfaces* **2022**, *14*, 15911−15926.
(21) Vinagreiro, C. S.; Zangirolami, A.; Schaberle, F. A.; Nunes, S. C. C.; Blanco, K. C.; Inada, N. M.; da Silva, G. J.; Pais, A.; Bagnato, V. S.; Arnaut, L. G.; Pereira, M. M. Antibacterial Photodynamic Inactivation of Antibiotic-Resistant Bacteria and Biofilms with Nanomolar Photosensitizer Concentrations. *ACS Infect. Dis.* **2020**, *6*, 1517−1526.
(22) Xi, J.; Wei, G.; Wu, Q.; Xu, Z.; Liu, Y.; Han, J.; Fan, L.; Gao, L. Light-enhanced sponge-like carbon nanozyme used for synergetic antibacterial therapy. *Biomater. Sci.* **2019**, *7*, 4131−4141.
(23) Xiao, F.; Cao, B.; Wen, L.; Su, Y.; Zhan, M.; Lu, L.; Hu, X. Photosensitizer conjugate-functionalized poly(hexamethylene guanidine) for potentiated broad-spectrum bacterial inhibition and enhanced biocompatibility. *Chin. Chem. Lett.* **2020**, *31*, 2516−2519.
(24) Zhang, X.; Zhang, Z.; Shu, Q.; Xu, C.; Zheng, Q.; Guo, Z.; Wang, C.; Hao, Z.; Liu, X.; Wang, G.; Yan, W.; Chen, H.; Lu, C. Copper Clusters: An Effective Antibacterial for Eradicating Multidrug-Resistant Bacterial Infection In Vitro and In Vivo. *Adv. Funct. Mater.* **2021**, *31*, 2008720.
(25) Zhao, X.; Chang, L.; Hu, Y.; Xu, S.; Liang, Z.; Ren, X.; Mei, X.; Chen, Z. Preparation of Photocatalytic and Antibacterial MOF Nanozyme Used for Infected Diabetic Wound Healing. *ACS Appl. Mater. Interfaces* **2022**, *14*, 18194−18208.
(26) Zhou, Q.; Lyu, X.; Cao, B.; Liu, X.; Liu, J.; Zhao, J.; Lu, S.; Zhan, M.; Hu, X. Fast Broad-Spectrum Staining and Photodynamic Inhibition of Pathogenic Microorganisms by a Water-Soluble Aggregation-Induced Emission Photosensitizer. *Front. Chem.* **2021**, *9*, 755419.
(27) Chen, Y.; Gao, Y.; Chen, Y.; Liu, L.; Mo, A.; Peng, Q. Nanomaterials-based photothermal therapy and its potentials in antibacterial treatment. *J. Controlled Release* **2020**, *328*, 251−262.
(28) Han, X.; Boix, G.; Balcerzak, M.; Moriones, O. H.; Cano-Sarabia, M.; Cortés, P.; Bastús, N.; Puntes, V.; Llagostera, M.; Imaz, I.; Maspoch, D. Antibacterial Films Based on MOF Composites that Release Iodine Passively or Upon Triggering by Near-Infrared Light. *Adv. Funct. Mater.* **2022**, *32*, 2112902.
(29) Li, C.; Li, Z.; Gan, Y.; Jiang, F.; Zhao, H.; Tan, J.; Yang, Y. Y.; Yuan, P.; Ding, X. Selective Capture, Separation, and Photothermal Inactivation of Methicillin-Resistant Staphylococcus aureus (MRSA) Using Functional Magnetic Nanoparticles. *ACS Appl. Mater. Interfaces* **2022**, *14*, 20566−20575.
(30) Wang, C.; Zhao, W.; Cao, B.; Wang, Z.; Zhou, Q.; Lu, S.; Lu, L.; Zhan, M.; Hu, X. Biofilm-Responsive Polymeric Nanoparticles with Self-Adaptive Deep Penetration for *In vivo* Photothermal Treatment of Implant Infection. *Chem. Mater.* **2020**, *32*, 7725−7738.
(31) Yu, S.; Li, G.; Zhao, P.; Cheng, Q.; He, Q.; Ma, D.; Xue, W. NIR-Laser-Controlled Hydrogen-Releasing PdH Nanohydride for Synergistic Hydrogen-Photothermal Antibacterial and Wound-Healing Therapies. *Adv. Funct. Mater.* **2019**, *29*, 1905697.
(32) Li, D.; Ushakova, E. V.; Rogach, A. L.; Qu, S. Optical Properties of Carbon Dots in the Deep-Red to Near-Infrared Region Are Attractive for Biomedical Applications. *Small* **2021**, *17*, No. e2102325.
(33) Aksoy, I.; Küçükkeçeci, H.; Sevgi, F.; Metin, O.; Hatay Patir, I. Photothermal antibacterial and antibiofilm activity of black phosphorus/gold nanocomposites against pathogenic bacteria. *ACS Appl. Mater. Interfaces* **2020**, *12*, 26822−26831.
(34) Jia, W.; Huang, F.; Zhang, Q.; Zhao, L.; Li, C.; Lu, Y. Novel conjugated small molecule-based nanoparticles for NIR-II photothermal antibacterial therapy. *Chem. Commun.* **2022**, *58*, 6340−6343.
(35) Li, J.; Li, Z.; Liu, X.; Li, C.; Zheng, Y.; Yeung, K. W. K.; Cui, Z.; Liang, Y.; Zhu, S.; Hu, W.; Qi, Y.; Zhang, T.; Wang, X.; Wu, S. Interfacial engineering of Bi2S3/Ti3C2Tx MXene based on work function for rapid photo-excited bacteria-killing. *Nat. Commun.* **2021**, *12*, 1224.

(36) Sun, J.; Song, L.; Fan, Y.; Tian, L.; Luan, S.; Niu, S.; Ren, L.; Ming, W.; Zhao, J. Synergistic Photodynamic and Photothermal Antibacterial Nanocomposite Membrane Triggered by Single NIR Light Source. *ACS Appl. Mater. Interfaces* **2019**, *11*, 26581−26589.
(37) Xu, J. W.; Yao, K.; Xu, Z. K. Nanomaterials with a photothermal effect for antibacterial activities: an overview. *Nanoscale* **2019**, *11*, 8680−8691.
(38) Zhang, L.; Wang, Y.; Wang, J.; Wang, Y.; Chen, A.; Wang, C.; Mo, W.; Li, Y.; Yuan, Q.; Zhang, Y. Photon-Responsive Antibacterial Nanoplatform for Synergistic Photothermal-/Pharmaco-Therapy of Skin Infection. *ACS Appl. Mater. Interfaces* **2019**, *11*, 300−310.
(39) Guo, Z.; Xie, W.; Lu, J.; Guo, X.; Xu, J.; Xu, W.; Chi, Y.; Takuya, N.; Wu, H.; Zhao, L. Tannic acid-based metal phenolic networks for bio-applications: a review. *J. Mater. Chem. B* **2021**, *9*, 4098−4110.
(40) Li, Y.; Miao, Y.; Yang, L.; Zhao, Y.; Wu, K.; Lu, Z.; Hu, Z.; Guo, J. Recent Advances in the Development and Antimicrobial Applications of Metal-Phenolic Networks. *Adv. Sci.* **2022**, *9*, No. e2202684.
(41) Xu, Y.; Xiao, L.; Chen, J.; Wu, Q.; Yu, W.; Zeng, W.; Shi, Y.; Lu, Y.; Liu, Y. $\alpha$-Fe2O3 based nanotherapeutics for near-infrared/dihydroartemisinin dual-augmented chemodynamic antibacterial therapy. *Acta Biomater.* **2022**, *150*, 367−379.
(42) Zhao, X.; Pei, D.; Yang, Y.; Xu, K.; Yu, J.; Zhang, Y.; Zhang, Q.; He, G.; Zhang, Y.; Li, A.; Cheng, Y.; Chen, X. Green Tea Derivative Driven Smart Hydrogels with Desired Functions for Chronic Diabetic Wound Treatment. *Adv. Funct. Mater.* **2021**, *31*, 2009442.
(43) Huang, Y. W.; Zhu, Q. Q.; Yang, X. Y.; Xu, H. H.; Sun, B.; Wang, X. J.; Sheng, J. Wound healing can be improved by (-)-epigallocatechin gallate through targeting Notch in streptozotocin-induced diabetic mice. *FASEB J.* **2019**, *33*, 953−964.
(44) Li, Q.; Xiao, W.; Zhang, F.; Liu, Q.; Ye, J.; Dong, H.; Cao, X. Tannic acid-derived metal-phenolic networks facilitate PCL nanofiber mesh vascularization by promoting the adhesion and spreading of endothelial cells. *J. Mater. Chem. B* **2018**, *6*, 2734−2738.
(45) Dong, R.; Zhang, H.; Guo, B. Emerging hemostatic materials for non-compressible hemorrhage control. *Natl. Sci. Rev.* **2022**, *9*, nwac162.
(46) Guo, B.; Dong, R.; Liang, Y.; Li, M. Haemostatic materials for wound healing applications. *Nat. Rev. Chem* **2021**, *5*, 773−791.


https://doi.org/10.1021/acsomega.2c07170
*ACS Omega* 2023, 8, 4889−4898